Computer Physics Communications 286 (2023) 108685

Contents lists available at ScienceDirect

Computer Physics Communications

journal homepage: www.elsevier.com/locate/cpc

Quasi-exact ground-state extrapolation for the random-field Potts model ☆

Manoj Kumar, Martin Weigel *

Institut für Physik, Technische Universität Chemnitz, 09107 Chemnitz, Germany

ARTICLE INFO

Article history:
Received 21 September 2022
Received in revised form 13 January 2023
Accepted 29 January 2023
Available online 1 February 2023

Keywords:
Potts model
Quenched disorder
Combinatorial optimization
Critical phenomena
Spin models
Ground states

ABSTRACT

The use of combinatorial optimization algorithms has contributed substantially to the major progress that has occurred in recent years in the understanding of the physics of disordered systems, such as the random-field Ising model. While for this system exact ground states can be computed efficiently in polynomial time, the related random-field Potts model is NP hard computationally. Hence, exact ground states cannot be computed for large systems in this case, but approximation schemes based on graph cuts and related techniques can be used. Here we show how a combination of such methods with repeated runs allows for a systematic extrapolation of relevant system properties to the ground state. The method is benchmarked on a special class of disorder samples for which exact ground states are available.

1. Introduction

Impurities are omnipresent in samples in the laboratory. Their theoretical description in terms of quenched random disorder in magnetic systems represented by spin models turns out to be an extremely challenging task that has attracted an extensive amount of research activity in past decades [1]. Disorder has profound effects on the type of ordering and the nature of the associated phase transitions. Much of the progress achieved to date towards an understanding of such systems has been due to large-scale numerical simulation efforts. Standard approaches such as canonical Monte Carlo simulations are heavily affected by the complex free-energy landscapes characterized by a multitude of metastable states separated by barriers that are the signature of such systems [2]. More sophisticated techniques in the form of generalized-ensemble simulations such as parallel tempering [3,4], multicanonical simulations [5–7] or, most recently, population annealing [8–12], lead to dramatically improved performance in such situations [13], but they are not able to fully remove the slowing down of dynamics induced by the combination of disorder and frustration.

For the case of random-field systems, where the renormalization group indicates that the fixed point relevant for the critical behavior sits at zero temperature [14], an alternative approach of analysis is based on the study of the ground states of individual disorder samples. To arrive at such configurations one might employ generic optimization methods such as simulated annealing [15] or genetic algorithms [16–18] that provide capabilities to overcome the inherent energy barriers and/or explore different valleys independently, but such techniques do not constitute a magic bullet for handling the complexity of the energy landscape. As was noted early on [19], for the random-field problem with Ising symmetry (RFIM) things are somewhat easier in that the ground-state computation can be mapped onto a maximum-flow problem for which efficient (polynomial-time) algorithms are available [20]. This has enabled high-precision analyses of the critical behavior of this model, see, e.g., Refs. [21–25].

For related, somewhat richer systems such as the random-field Potts model (RFPM), however, the situation is less fortunate as the ground-state problem for more than two spin states corresponds to optimizing a multi-terminal flow, a task that can be shown to be NP hard, even in two dimensions [26]. While it is hence not possible for this system to find exact ground states in polynomial time, we have shown recently that good approximations can be computed with reasonable time investment employing suitable generalizations of the graph-cut (GC) methods used for the RFIM [27]. Algorithms for this purpose have previously been discussed in the context of computer vision [28]. In the following, we investigate how a randomization of this approach allows one to construct an extension that systematically converges to the exact ground state. By constructing a particular set of disorder samples

☆ The review of this paper was arranged by Prof. Blum Volker.

* Corresponding author.
E-mail addresses: manojkmr8788@gmail.com (M. Kumar), martin.weigel@physik.tu-chemnitz.de (M. Weigel).

https://doi.org/10.1016/j.cpc.2023.108685
0010-4655/

for which exact results are available from a different approach (TRW-S as proposed in Ref. [29]), we study how the minimum energies as well as state overlaps of the randomized method approach the exact result, thus developing a technique for systematic extrapolation of the approximate data.

The remainder of this paper is organized as follows. In Sec. 2 we define the random-field Potts model in the variant discussed here and describe the graph-cut technique for computing approximate ground states. We then discuss how n repeated runs with different initial conditions are used for a systematic improvement of results. This leads to n-dependent estimates of the thermodynamic quantities that are later used for extrapolation. In addition, we introduce the TRW-S method that allows us to generate a set of samples with the associated exact ground states. In Sec. 3 we compare the TRW-S and graph-cut algorithms and report on our results for the extrapolation of approximate ground states. A detailed analysis of exact samples reveals that typical quantities approach their ground-state values in a double power-law fashion that is also shown to apply to the case of regular samples. This setup enables a reliable extrapolation of data for moderate values of n to the $n \to \infty$ limit. Finally, Sec. 4 contains our conclusions.

2. Model and methodology

2.1. The random-field Potts model and graph cuts

The q-state RFPM considered here is governed by the Hamiltonian [30]

$$\mathcal{H} = -J \sum_{\langle ij \rangle} \delta_{s_i,s_j} - \sum_i \sum_{\alpha=0}^{q-1} h_i^\alpha \delta_{s_i,\alpha}, \tag{1}$$

where $\delta_{x,y}$ is the Kronecker delta function. According to the Potts symmetry, the spins s_i take values from the set $\{0, 1, ..., q-1\}$. The variables $\{h_i^\alpha\}$ are the quenched random fields at site i, acting on state α, and each is drawn independently from a normal distribution,

$$P(h_i^\alpha) = \frac{1}{\sqrt{2\pi}\,\Delta} \exp\left[-\frac{(h_i^\alpha)^2}{2\Delta^2}\right]. \tag{2}$$

The standard deviation Δ determines the strength of disorder. Different ways of exposing the Potts spins to random fields have also been considered [31,32], especially for the case of discrete random-field distributions. While we did not consider such variations explicitly, we expect the general results discussed in the present study to carry over to such generalized disorder distributions.

For $q = 2$, it can be easily seen that the RFPM Hamiltonian in Eq. (1) corresponds to the RFIM. In this case, $\mathcal{H}$ can be written as [27],

$$\begin{aligned}\mathcal{H} = &-\frac{J}{2}\sum_{\langle ij \rangle}[\sigma_i\sigma_j + 1] \\ &-\frac{1}{2}\sum_i [(h_i^+ - h_i^-)\sigma_i + (h_i^+ + h_i^-)],\end{aligned} \tag{3}$$

where h_i^+ and h_i^- represent the two field components with $\alpha = \pm$ according to Eq. (1), and $\sigma_i = \pm 1$ are Ising spins. The problem hence corresponds to the RFIM at coupling $J/2$ and field strength $\Delta/\sqrt{2}$. In this case, the task of finding ground states is equivalent to finding a minimum (s,t) cut that partitions the graph into two disjoint sets of nodes: one that has spins down (including s) and one with spins up (including t) [19,33]. Here, s and t are ghost vertices relating to positive and negative random magnetic fields, respectively. Such minimum cuts can be found in a time polynomial in the number of sites based on the min-cut/max-flow correspondence [34], by using algorithms such as Ford-Fulkerson or push-relabel for the flow problem [28].

For $q > 2$, on the other hand, the problem of finding ground states is NP hard [26]. Nevertheless, a graph-cut approach for fast approximate minimization of such energy functions, occurring in computer vision problems, was proposed by Boykov et al. [26], and later on developed into an approximate ground-state algorithm for the RFPM in Ref. [27]. The basic idea amounts to the embedding of an Ising symmetry into the Potts model, such that exact algorithms can be used to solve a partial problem. Two variants of this idea were proposed in Ref. [26], dubbed α-β-swap and α-expansion. For the α-β-swap, two spin orientations or *labels* $\alpha \neq \beta \in \{0, 1, ..., q-1\}$ are picked and all labels apart from α and β are frozen; the update consists of a swap of the labels between regions. In contrast, for α-expansion one picks a label α and attempts to expand it while freezing all the remaining labels, cycling through the labels in turn in q iterations. The structure of this algorithm can be described as follows:

```
procedure GraphCutMethodExpansion({s_i})
    initialize {s_i} at random
    set success = True
    while success == True do
        success = False
        for each α ∈ {0, 1, ..., q − 1} do
            find {ŝ_i} = arg min H({s'_i}) among {s'_i}
                 within one α-expansion of {s_i}
            if H({ŝ_i}) < H({s_i}), set {s_i} = {s'_i}
                 and success = True
        end for
    end while
    return {s_i}
end procedure
```

While for the α-β swap, one has:

```
procedure GraphCutMethodSwap({s_i})
    initialize {s_i} at random
    set success = True
    while success == True do
        success = False
        for each pair (α, β) ⊂ {0, 1, ..., q − 1} do
            find {ŝ_i} = arg min H({s'_i}) among {s'_i}
                 within one α-β swap of {s_i}
            if H({ŝ_i}) < H({s_i}), set {s_i} = {s'_i}
                 and success = True
        end for
    end while
    return {s_i}
end procedure
```

Both methods correspond to downhill optimization techniques, but with a highly non-local move set, such that many (but not all) metastable states are avoided. In practice, we focus on the α-expansion move as this is found to be somewhat more efficient for our problem. For a more detailed discussion of these minimization techniques see Refs. [26–28].

2.2. Ground-state extrapolation

For a fixed disorder sample $\{h_i^\alpha\}$, applying q iterations of α-expansion provides a metastable minimum or candidate ground state. By nature of the approach, this state also depends on the

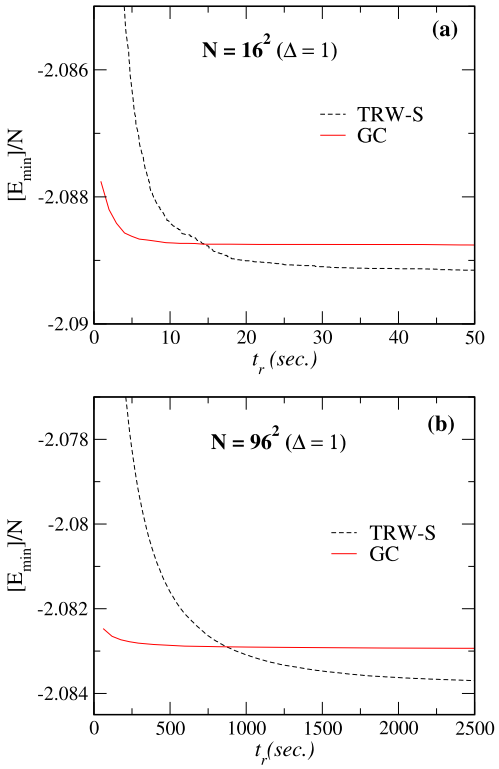

Fig. 1. Plots of the disorder-averaged approximate ground-state energies, $[E_{\min}]/N$, of the $q = 3$ RFPM as a function of run-time t_r for TRW-S and GC on 2D square lattices (coordination number $z = 4$). Panel (a) is for system size $N = 16^2$ whereas panel (b) is for $N = 96^2$. The data are averaged over 1000 random-field realizations.

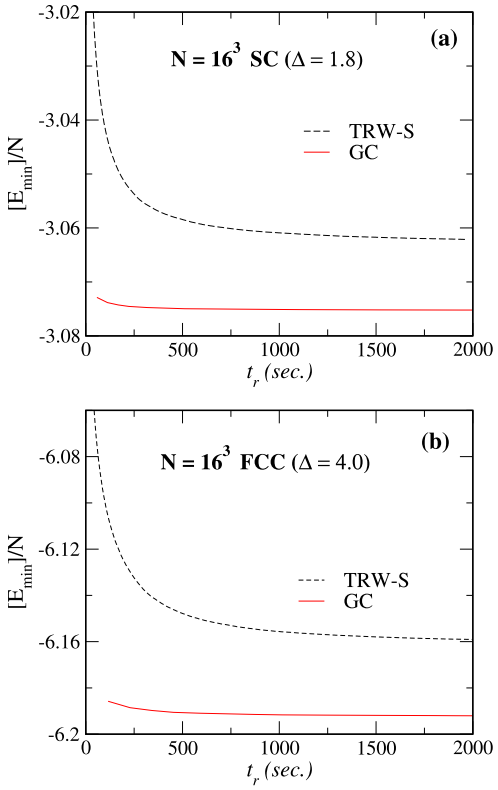

Fig. 2. The same as Fig. 1 but for systems on three-dimensional lattices. Panel (a) is for the 16^3 RFPM system on a simple cubic lattice ($z = 6$) whereas panel (b) is for the same system but on a face-centered cubic lattice ($z = 12$).

initial configuration of spins $\{s_i^I\}$. Hence a strategy for further improving the minimization results consists of performing repeated runs for several initial configurations and picking the run resulting in the lowest energy. If the probability of finding the exact ground state in one run is $P_0(\{h_i^\alpha\})$, the success probability for n runs increases exponentially [18,27],

$$P_s(\{h_i^\alpha\}) = 1 - [1 - P_0(\{h_i^\alpha\})]^n, \tag{4}$$

such that the method becomes exact in the limit $n \to \infty$. This is also evident from the following observation: if one tries all possible q^N initial conditions in this way (where N is the total number of spins), the monotonous nature of α-expansion guarantees that (at least) the run starting with the ground-state $\{s_i^0\}$ as an initial condition will also end in the ground state. It is hence justified to extrapolate the relevant disorder averages in n to probe the true ground-state behavior. As we will see below, however, our numerical calculations are not in the asymptotic regime where the exponential convergence of Eq. (4) is visible, and instead we find the power-law form of Eq. (10) to correctly describe the data.

As a consequence of such a procedure, we consider n-dependent averages of the relevant observables, focusing on the following quantities: the magnetic order parameter [35]

$$m(n) = \frac{q\rho - 1}{q - 1}, \tag{5}$$

where

$$\rho(n) = \frac{1}{N} \max_\alpha \left(\sum_i \delta_{s_i,\alpha} \right) \tag{6}$$

is the fraction of spins in the preferred orientation; the bond energy

$$e_J(n) = -\frac{1}{N} \sum_{\langle ij \rangle} \delta_{s_i,s_j}, \tag{7}$$

as well as the relative deviation from the ground-state energy E_0,

$$\varepsilon(n) = \frac{E_0 - E}{E_0}, \tag{8}$$

where $E = \mathcal{H}(\{s_i\})$, which we call the *accuracy* of the approximation; and, finally, the ground-state overlap,

$$o(n) = \frac{1}{N} \sum_i \delta_{s_i,s_i^0}, \tag{9}$$

where $\{s_i^0\}$ denotes the ground-state spin configuration.

In order to evaluate ε and o and, more generally, to judge the quality of approximation, it is crucial to have access to a set of samples for which ground states are known. Such samples are, in general, hard to come by for any non-trivial system size. Here, we make use of an alternative minimization algorithm, the sequential tree-reweighted message passing (TRW-S) method proposed by Kolmogorov [29,36] which, formally, amounts to solving the dual of the linear program defined by Eq. (1), such that in addition to the proposed spin configuration of decreasing minimal energy it also provides an increasing lower bound on the ground-state energy. While the bound is normally distinct from the energy of the proposed configuration, the proposed state must be the exact ground state in case the two energies coincide. (Note that this is a sufficient, but not a necessary condition for TRW-S to have found the ground state.) We ran TRW-S on many samples to select a subset for which this condition was met and we hence can be sure of having found the exact ground state; in the following, we refer to these as *exact samples*. They were then used for benchmarking the technique of multiple runs with α-relaxation outlined above. Below, we also present numerical results for *regular samples* for which

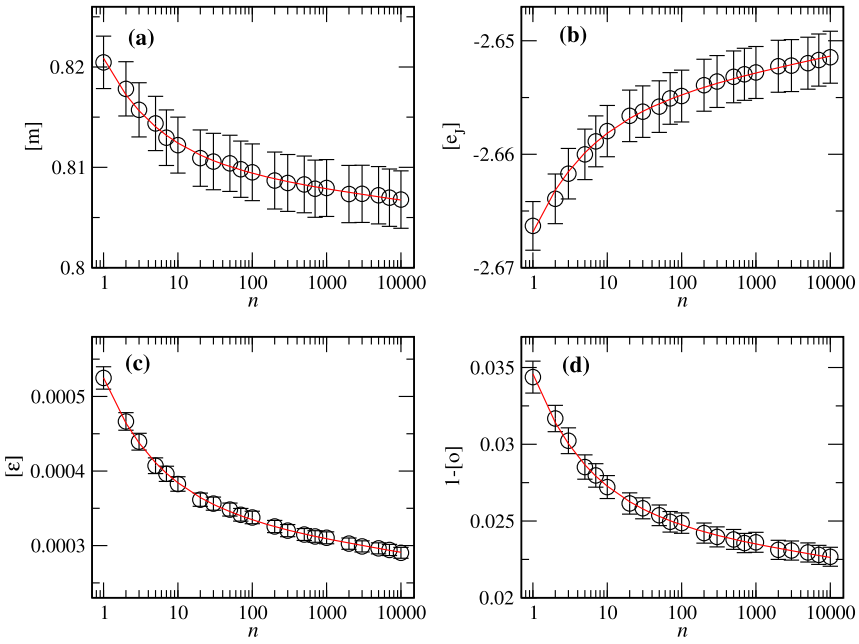

Fig. 3. Disorder-averaged estimates of (a) the magnetization $[m]$, (b) the bond energy $[e_J]$, (c) the accuracy $[\varepsilon]$, and (d) the residual overlap $1-[o]$ of approximate ground states found from α-expansion on "exact" disorder samples of the $q=3$ RFPM with $N=16^3$ spins as a function of the number n of initial conditions used. The red lines correspond to joint fits of the non-linear form of Eq. (10) to the data for all four observables.

the exact solutions are not known. As we shall see, the statistical properties of exact samples are distinct from but still sufficiently similar to those of the regular ensemble; a detailed discussion of this aspect appears in Sec. 3.2.2.

3. Numerical results

3.1. Graph cuts and tree-reweighted message passing

Let us begin by comparing the two approximation algorithms: TRW-S and the α-expansion GC. Unlike GC, the TRW-S method does not take into account the initial spin labeling. Instead, TRW-S is a probabilistic message passing algorithm where an iteration corresponds to the passing of a message for each bond. As such, it converges much more slowly to a solution than the graph-cut approach for a single initial spin configuration (and it might require damping to even converge at all [29]), but the resulting individual minima are in some cases lower than those found by graph cuts for a single initial labeling. The power of graph cuts results from the possibility of iterating over different initial labellings according to Eq. (4). For the TRW-S method, we hence obtain approximate ground states of improving quality on increasing the number of iterations i, while for GC results improve with increasing numbers n of initial labellings. In order to compare their performance, we ran both techniques for the same set of 1000 distinct disorder samples, and determined the energies $E_{\min}$ of the lowest-state in i iterations of TRW-S or n labellings of GC, where n and i were chosen to result in the same CPU time t_r (in seconds).

Fig. 1 shows plots of disorder-averaged minimal energies $E_{\min}$ per spin, i.e. $[E_{\min}]/N$, as a function of run-time t_r for samples of the two-dimensional $q=3$ RFPM on square lattices of sizes $N=16^2$ (panel a) and $N=96^2$ (panel b), respectively. The disorder samples are drawn at $\Delta=1$, which corresponds to quite strong disorder in two dimensions [27]. It is clear from both panels that initially GC finds states of lower energy than TRW-S, but with increasing run-time there is a crossover and eventually TRW-S performs better than GC. Another observation is that in contrast to TRW-S, GC quickly produces better approximate solutions, which then improve only slowly with the run-time. These findings are consistent with the study of Kolmogorov [29], who compared these techniques for a stereo matching problem.

Next, in Fig. 2, we compare these techniques for the case of three-dimensional lattices. Panel (a) shows the comparison for a 16^3 $q=3$ RFPM on a *simple-cubic* (SC) lattice for which the coordination number $z=6$, whereas panel (b) shows the comparison for the same system size on a *face-centered cubic* (FCC) lattice, where each spin is linked to 12 nearest neighbors via the coupling strength J (i.e., $z=12$). The disorder strength Δ is chosen in both cases to be in the strong-disorder regime. In particular, we use $\Delta=1.8$ for SC and $\Delta=4.0$ for FCC. As is clearly seen from Fig. 2, GC performs better than TRW-S in both of these cases. This observation is in line with previous work by Kolmogorov and Rother [37] who compared such techniques on vision problems for highly connected graphs. Specifically, they tested the energy minimization algorithms for stereo problems with occlusions and found that the speed of convergence of TRW-S becomes slower as the connectivity increases, and for graphs with $z>4$ GC outperforms TRW-S. In the following, we hence focus on the use of the GC approach for our target problem of the RFPM in three dimensions.

3.2. Extrapolation to the quasi-exact limit

In the following, we study the three-dimensional RFPM for $q=3$ and $q=4$, respectively, at first focusing on ground-state extrapolation for simple cubic systems of size $N=16^3$ that are large enough to provide a non-trivial benchmark of the ground states for the α-expansion GC approach [27].

3.2.1. Exact samples

In order to generate a sample set for benchmarking, we first ran TRW-S for 10^4 iterations per random-field configuration and searched for exact samples for which the minimum energy $E_{\min}$ of the spin configuration becomes equal to the lower bound E_b on the ground-states. For $q=3$, out of 2×10^5 disorder samples at $\Delta=1.8$ we found 1368 samples with exact ground states. For $q=4$ at $\Delta=1.7$, on the other hand, 1530 out of 2×10^6 disorder samples had a tight lower bound. Note that these values of the

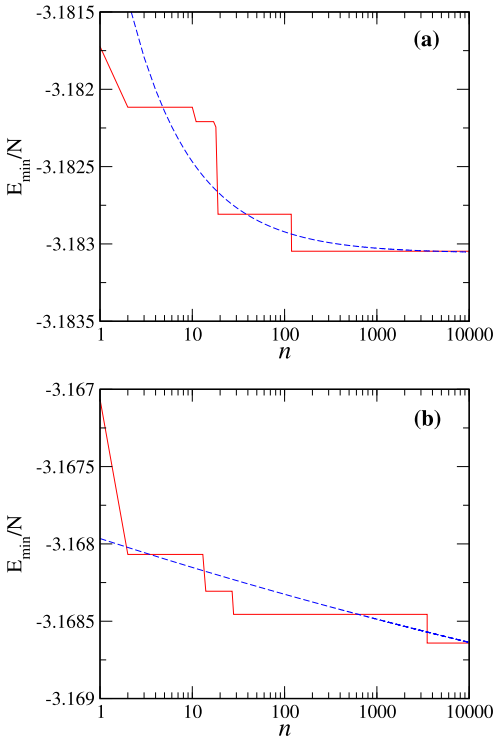

Fig. 4. Plots of $E_{\min}/N$ versus n for two different samples at $\Delta = 1.8$. The continuous dashed curves are fits of the form $E_{\min} = a_0 n^{-a_1} + E_0$ to the data. The values of fit parameters in panel (a) are $a_1 = 0.633$, $E_0 = -3.18306$, and in panel (b) $a_1 = 0.0321$, $E_0 = -3.1686$.

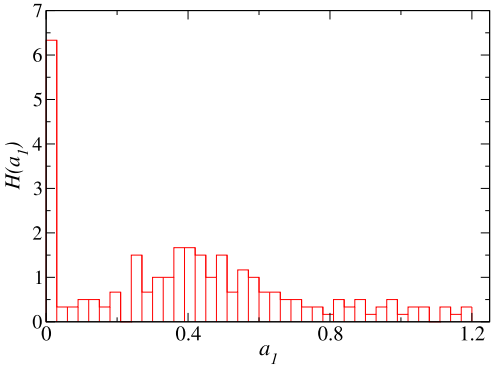

Fig. 5. Histogram of 200 values of the power-law exponent a_1 according to the functional form $E_{\min} = a_0 n^{-a_1} + E_0$ used for fitting $E_{\min}(n)$ of individual samples according to Fig. 4.

random-field strength are in the disordered phase slightly above the transition.

We then ran the α-expansion algorithm for these exact samples, using up to $n_{\max} = 10\,000$ different initial conditions for each random-field configuration. From the state of lowest energy among n runs, we determined the observables defined in Eqs. (5)–(9). For all $n \le n_{\max}$, these quantities were then averaged over the total number of (exact) disorder samples $N_{\text{samp}} = 1368$ for $q = 3$ and $N_{\text{samp}} = 1530$ for $q = 4$, respectively. Error bars on all estimates were determined from the sample-to-sample fluctuations.

Fig. 3 shows the disorder averaged quantities $[m]$, $[e_J]$, $[\varepsilon]$, and $1 - [o]$ of Eqs. (5)–(9) as a function of n for the $q = 3$ case. We find that the convergence of all averages is well described by the same power-law form,

$$\mathcal{O}(n) = a n^{-b}(1 + c n^{-d}) + \mathcal{O}^*, \tag{10}$$

where $\mathcal{O}^*$ is the asymptotic value of the quantity denoted as $\mathcal{O}$. Besides the leading power law n^{-b}, we observe a power-law correction with exponent d. In the following, we present some of the evidence that justifies and explains the scaling form of Eq. (10).

We analyzed the convergence of $E_{\min}$ with respect to n of α-expansion for 200 individual disorder samples and found two kinds of behavior: one in which $E_{\min}$ decays markedly with n and then converges, say, to E_0 for $n \to \infty$, and the other where it converges very slowly in n. The first behavior appears due to those samples for which the approximate solutions found initially are far from the exact solutions, and hence such estimates improve considerably for lower n before saturating to the exact solutions (E_0) or until they arrive in the proximity of E_0, after which they start converging slowly with increasing n, whereas the other behavior would be due to those samples for which the initial approximations are near to the exact solutions and hence they show overall a slow convergence in n. In Fig. 4, we show a typical plot of such convergences for two different kinds of samples. Notice the behavior of $E_{\min}/N$ with varying n, shown by the solid lines. In panel (a), $E_{\min}$ is decaying considerably already for smaller n as compared to panel (b). The smooth dashed curves are fits of the form $E_{\min} = a_0 n^{-a_1} + E_0$ to the data. The value of the exponent a_1 in panel (a) is 0.633 and in panel (b) it is 0.032. In Fig. 5 we show a histogram of 200 values of a_1. In this figure, the histogram clearly peaks in two different regimes; one in which the value of a_1 is small ($\lesssim 0.05$) and the other regime corresponds to larger value of a_1. Combining the two different power-law regimes containing a smaller and a larger value of a_1 justifies our full functional form of convergence in Eq. (10), in which the exponent b corresponds to the asymptotic exponent for slow convergence in n whereas the exponent d is responsible for the fast decay of observable estimates for smaller values of n.

Coming back to Fig. 3, we show the result of a joint fit of this form to the data for all four observables, where the exponents b and d are constrained to share the same value among all observables, while the amplitudes a and c are allowed to differ for different $\mathcal{O}$. The quality of fit is $Q \approx 1$. (Note that the data for different n are for the same random-field samples and hence statistically correlated, but see below for the behavior for uncorrelated samples.) The resulting fits are shown together with the data in Fig. 3, and it is seen that they model the data extremely well. The extrapolated values of all quantities, corresponding to $\mathcal{O}^*$ in Eq. (10), together with the exact values $\mathcal{O}_{\text{ex}}$ are summarized in Table 1. Clearly the extrapolated and exact results are consistent. The power-law exponents are found to be $b \simeq 0.03$ for the leading, and $d \simeq 0.56$ for the correction exponent. We point out that the occurrence of two types of convergence behaviors for different samples as illustrated in Fig. 5 is an empirical observation that justifies our scaling form (10), but to understand its fundamental

Table 1
Extrapolated ($\mathcal{O}^*$) and exact ($\mathcal{O}_{\text{ex}}$) results for the observable values of Eqs. (5)–(9) for the exact samples for $q = 3$, $\Delta = 1.8$ and $q = 4$, $\Delta = 1.7$. The numbers in parentheses are the error estimates on the last significant figures. These error bars are calculated from fits with the exponents of Eq. (10) fixed to their values found from the unconstrained fit.

q	$[m]^*$	$[m]_{\text{ex}}$	$[e_J]^*$	$[e_J]_{\text{ex}}$	$[\varepsilon]^*$	$[\varepsilon]_{\text{ex}}$	$1-[o]^*$	$1-[o]_{\text{ex}}$
3	0.793(14)	0.780(3)	−2.63(2)	−2.615(3)	0.000065(72)	0	0.012(13)	0
4	0.86(2)	0.866(2)	−2.653(27)	−2.673(2)	0.00013(15)	0	0.005(9)	0

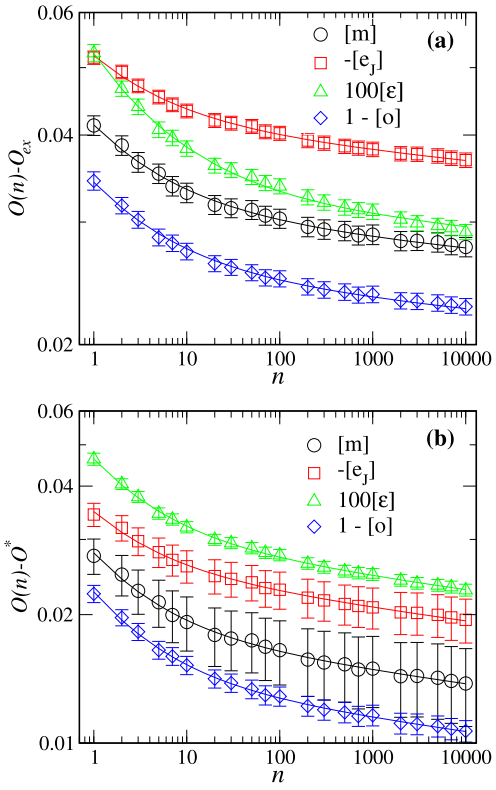

Fig. 6. Residuals of the observables of Eqs. (5), (8), and (9) for the $q = 3$ RFPM as a function of the number of initial conditions n relative to (a) the exact results $\mathcal{O}_{\rm ex}$, and (b) the extrapolated results $\mathcal{O}^*$. The solid lines correspond to joint fits of the form (10) to the data for the different observables, taking a, b, c and d as parameters.

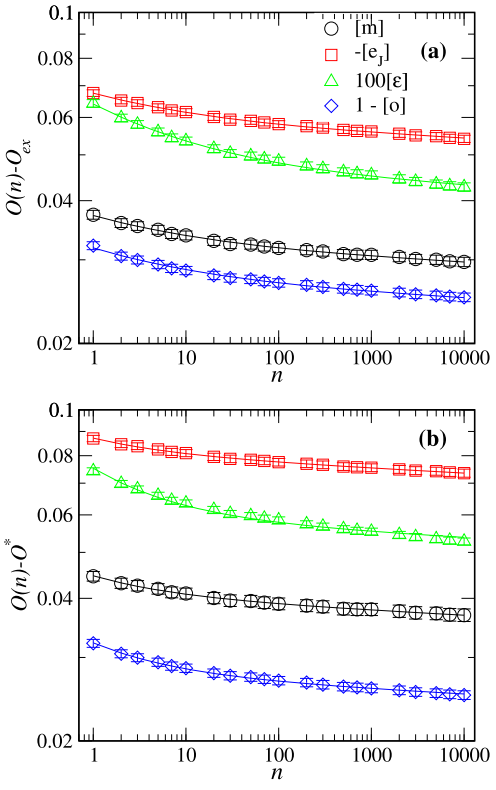

Fig. 7. Analogous to Fig. 6, but for $q = 4$.

origin would require a detailed model of the spacing and multiplicity of metastable states in the problem which is unfortunately not available. We also tried an alternative scaling form describing a logarithmic convergence to the ground state. Although this also led to acceptable fits to the data, the resulting values of O^* were not consistent with the values $O_{\rm ex}$ for the exact samples, thus invalidating this approach.

In Fig. 6, we plot the residuals of all quantities as a function of n. Panel (a) show the residuals with respect to the exact results, i.e., $\mathcal{O}(n) - \mathcal{O}_{\rm ex}$, in a log-log scale. For large n, these decay with n in a power-law fashion $\sim an^{-b}$. However, the data for small n clearly deviate from the power-law behavior, indicating the presence of scaling corrections. This again justifies the functional form of Eq. (10) for describing the data, where for the values shown in Fig. 6(b) the limiting value $\mathcal{O}^*$ is taken as a constant derived from the fits shown in Fig. 3 and not a fit parameter. Performing a joint fit to the four observables including all n as shown by the solid curves in Fig. 6, we arrive at the exponent values $b = 0.013 \pm 0.005$, and $d = 0.47 \pm 0.07$ for panel (a). Panel (b) shows residuals using the extrapolated results $\mathcal{O}^*$, determined in Fig. 3. Clearly the data fit very well to the form $an^{-b}(1 + cn^{-d})$, as shown by the solid curves. The exponents $b \simeq 0.03$ and $d = 0.56 \pm 0.12$ from the extrapolated fit agree with those of the fit using the exact results as shown in (a).

To check for the robustness of our approach regarding a variation in the number of states q, in Fig. 7 we show the residuals for $q = 4$. Again we consider two types of residuals: (a) using the exact ground states, (b) using extrapolated results. Also in this case, we find that the data is consistent with the behavior $an^{-b}(1 + cn^{-d})$, as shown by the solid curves. The fit in panel (a) yields the exponent $b = 0.009 \pm 0.005$ and $d = 0.32 \pm 0.07$. The extrapolated fit in panel (b) yields the exponents $b \simeq 0.01$ and $d = 0.48 \pm 0.16$, consistent with the fit enforcing convergence to the exact result shown in panel (a). The extrapolated estimates $\mathcal{O}^*$ are summarized in Table 1 and agree with the corresponding exact values.

3.2.2. Regular samples

Encouraged by the observed consistency in behavior for the ensemble of exact samples, we also considered the extrapolation behavior for the regular ensemble, for which exact solutions are not available. Here we naturally cannot consider the quantities ε and o, and we hence focus on m and e_J only. For consistency, we generated the same numbers $N_{\rm samp} = 1368$ ($q = 3$) and 1530 ($q = 4$) of regular disorder samples as we had previously considered for the exact samples. Also, in this case, we study various system sizes $N = L^3$ in order to resolve a potential system-size dependence of the scaling form (10). From this form, for a given N, if one plots $n^b[\mathcal{O}(n) - \mathcal{O}^*]$ as a function of n^{-d}, the data should fall on a straight line of intercept a and slope ac. This is what we show in Fig. 8 for the $q = 3$ RFPM, where the functional form (10) is used for joint fits of the data for $[m]$ and $[e_J]$ for each N, using common values of the exponents b and d, but allowing for different amplitudes a and c. Plotting the data in this way is useful to identify any deviations from the scaling form (10), especially in the asymptotic limit $n \to \infty$. Such deviations are not visible in our data, however, and they fit very well both for $[m]$ and $[e_J]$, and for different system sizes, as shown by the straight lines. The fit quality $Q \approx 1$ for all N. In Fig. 9, we next show the same behavior for the $q = 4$ RFPM and for different system sizes. Here, we also do not see any deviations from the scaling form (10). These results hence illustrate the robustness of our approach of extrapolation in the q-state RFPM as well as its applicability to systems of different size. The extrapolated values of the observables $[m]^*$ and $[e_J]^*$, together with the exponents b and d for both $q = 3$ and 4, and for different system sizes N are collected in Table 2. If we compare the extrapolated estimates corresponding to $N = 16^3$ to those for the exact samples given in Table 1, the values clearly dif-

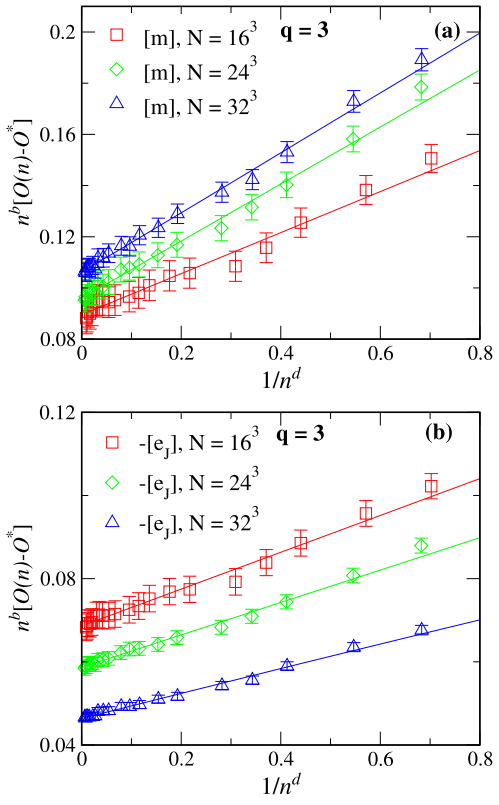

Fig. 8. Plot of $n^b[\mathcal{O}(n) - \mathcal{O}^*]$ as a function of n^{-d} according to the scaling form (10) for the data of magnetization m [panel(a)] and bond-energy e_J [panel(b)] for regular disorder samples of the $q = 3$ RFPM for different sizes $N = 16^3$, 24^3, and 32^3. The solid lines indicate the fits according to Eq. (10).

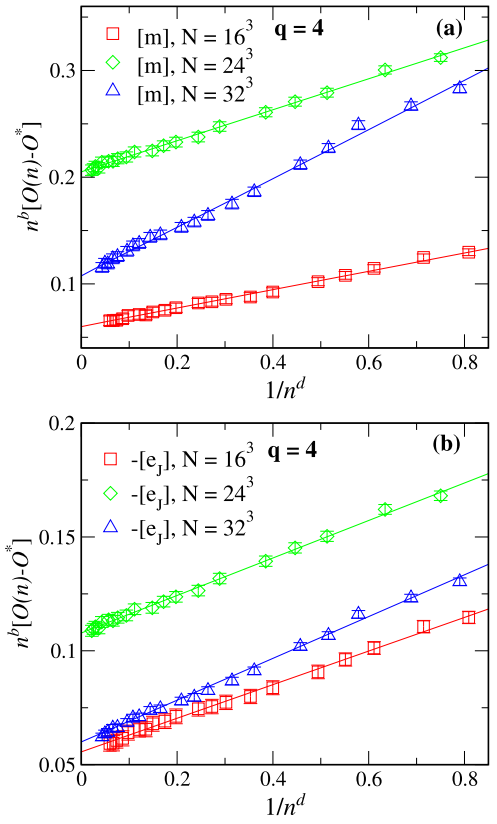

Fig. 9. Analogous to Fig. 8, but for $q = 4$.

fer between the exact and regular ensembles, and one might hence wonder how representative the exact samples are for the regular case. To enable a better judgment of this aspect, we considered the approach of our algorithm to the lowest-lying states in both ensembles as quantified by the *success probability*.

This is computed as follows: for each disorder sample of the exact and regular ensembles we run our expansion algorithm for a maximum of $n_{\max} = 10\,000$ initial conditions and check if the lowest-energy state is ever found in $n < n_{\max}$ runs. The success probability $P_s(n)$ is then estimated as the fraction of samples for which this state is found within n initial conditions. (Note that the runs for each value of n use independent initial configurations.) In this process, the lowest-energy state is defined as the state of lowest energy among *all* runs conducted for the sample. In Fig. 10, we show the plot of P_s against n for exact and regular ensembles of system size $N = 16^3$. It is clear from this figure that such lowest-energy states are found somewhat more easily for the exact than for the regular samples. However, with increasing n, there is a clear trend that P_s for the regular case converges to the behavior for the exact ensemble, thus supporting our previous finding of a consistent approach of the graph-cut estimates in both ensembles to the ground state.

So far the numerical results we presented are correlated in the sense that the same disorder samples are used for different values of n. Relaxing this assumption, in Fig. 11, we change the samples with varying n for a 16^3 RFPM, and consider the residuals $\mathcal{O}(n) - \mathcal{O}^*$ of $[m]$ and $[e_J]$ as a function of n for both $q = 3$ and 4. This is shown for the case of regular samples as we only have a limited number of exact samples. The data of $[m]$ and $[e_J]$ is used for a joint fit of the extrapolating form (10) as shown by the solid curves. The best fit yields the parameters $b \simeq 0.023, d = 0.71 \pm 0.15, [m]^* = 0.45 \pm 0.03, [e]^* = -2.417 \pm 0.017$ with a quality of fit $Q = 0.98$ for $q = 3$, and $b \simeq 0.01, d = 0.311 \pm 0.087, [m]^* = 0.697 \pm 0.084, [e]^* = -2.536 \pm 0.066$ with a quality of fit $Q = 0.56$ for $q = 4$. Comparing these fit results with those corresponding to $N = 16^3$ in Table 2, where the same samples are used for different n, we find that the exponents b and d slightly differ, but more importantly, the extrapolated observables $[m]^*$ and $[e]^*$ agree very well. This clearly manifests the robustness of our scaling form (10) for the extrapolation also for uncorrelated samples.

4. Summary and discussion

We have studied the performance of approximate ground-state algorithms based on graph cuts for the three-dimensional random-field Potts model. Combining the α-expansion approach developed in computer vision [26] with the use of repeated runs for different initial spin configurations [18,27] allows us to systematically improve the quality of approximation and the results must ultimately converge to the exact ground states as the number of

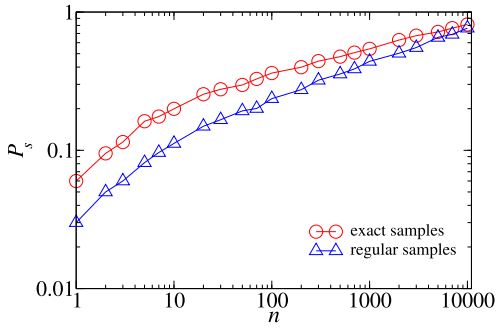

Fig. 10. Success probabilities $P_s(n)$ for the exact and regular ensembles, *i.e.*, the fraction of samples for which the lowest known state is found at least once in n runs. Here, $N = 16^3$.

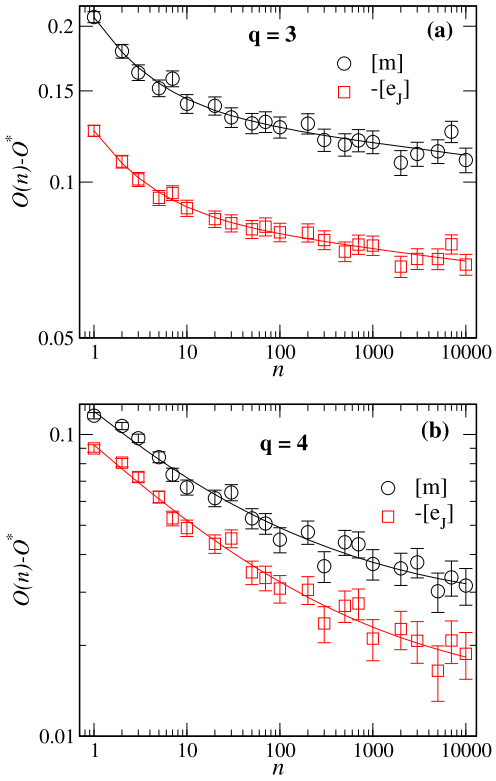

Fig. 11. Residual of the magnetization m and bond-energy e_J as a function of n for $q = 3$ [panel (a)] and for $q = 4$ [panel (b)] for regular disorder samples of the 16^3 RFPM, where samples are also changed in changing the value of n. The solid lines show joint fits of the form $an^{-b}(1 + cn^{-d})$ to the data.

initial conditions is increased. We provide the code for computing and analyzing RFPM ground states in this manner in a public repository [38]. Using a collection of samples of size 16^3 for which exact ground states for $q = 3$ and $q = 4$ are available from the TRW-S primal-dual optimization algorithm proposed by Kolmogorov [29,36] allowed us to illustrate the convergence explicitly. Comparing TRW-S to graph cuts, we find that the former algorithm has some advantages for weakly connected graphs as exemplified by the square lattice, but graph cuts outperform TRW-S for higher connectivities such as for lattices in three dimensions. Studying the behavior of the magnetization and bond energy as well as the deviation from the ground-state configuration and energy, we found that these quantities approach their exact values in a power-law fashion with an exponent that is common between different quantities. Using joint fits and incorporating a power-law scaling correction we found that our proposed scaling form fits the data very well, and the asymptotic values of all quantities in the limit of $n \to \infty$ agree with the exact results both for $q = 3$ as well as $q = 4$, see Table 1. For the case of regular samples that are most relevant for the practical task of extrapolating results of the α-expansion approach for larger systems we find a scaling behavior similar to that for the exact samples, thereby providing confidence that the extrapolation procedure outlined here will lead to reliable results for studying the critical behavior of the random-field Potts model more generally [39].

Declaration of competing interest

The authors declare that they have no known competing financial interests or personal relationships that could have appeared to influence the work reported in this paper.

Data availability

Data will be made available on request.

Acknowledgement

The authors acknowledge support by the Royal Society - SERB Newton International Fellowship (NIF\R1\180386). We acknowledge the provision of computing time on the parallel compute cluster Zeus of Coventry University.

References

[1] A.P. Young (Ed.), Spin Glasses and Random Fields, World Scientific, Singapore, 1997.
[2] W. Janke (Ed.), Rugged Free Energy Landscapes – Common Computational Approaches to Spin Glasses, Structural Glasses and Biological Macromolecules, Lect. Notes Phys., vol. 736, Springer, Berlin, 2007.
[3] C.J. Geyer, in: Computing Science and Statistics: Proceedings of the 23rd Symposium on the Interface, American Statistical Association, New York, 1991, pp. 156–163.
[4] K. Hukushima, K. Nemoto, J. Phys. Soc. Jpn. 65 (1996) 1604–1608.
[5] B.A. Berg, T. Neuhaus, Phys. Rev. Lett. 68 (1992) 9–12.
[6] W. Janke, in: B. Dünweg, D.P. Landau, A.I. Milchev (Eds.), Computer Simulations of Surfaces and Interfaces, in: NATO Science Series, II. Mathematics, Physics and Chemistry, vol. 114, Kluwer, Dordrecht, 2003, pp. 137–157.
[7] J. Gross, J. Zierenberg, M. Weigel, W. Janke, Comput. Phys. Commun. 224 (2018) 387–395.
[8] K. Hukushima, Y. Iba, AIP Conf. Proc. 690 (2003) 200–206.
[9] J. Machta, Phys. Rev. E 82 (2010) 026704.
[10] W. Wang, J. Machta, H.G. Katzgraber, Phys. Rev. E 92 (2015) 063307.
[11] L.Y. Barash, M. Weigel, M. Borovský, W. Janke, L.N. Shchur, Comput. Phys. Commun. 220 (2017) 341–350.
[12] M. Weigel, L.Y. Barash, L.N. Shchur, W. Janke, Phys. Rev. E 103 (2021) 053301.
[13] R. Kumar, J. Gross, W. Janke, M. Weigel, Eur. Phys. J. B 93 (5) (2020) 1–13.
[14] A.J. Bray, M.A. Moore, J. Phys. C 18 (28) (1985) L927.
[15] S. Kirkpatrick, C.D. Gelatt, M.P. Vecchi, Science 220 (1983) 671–680.
[16] P. Sutton, S. Boyden, Am. J. Phys. 62 (6) (1994) 549–552.
[17] M. Weigel, M.J.P. Gingras, Phys. Rev. Lett. 96 (2006) 097206.
[18] M. Weigel, Phys. Rev. E 76 (2007) 066706.
[19] J.C. Anglès d'Auriac, M. Preissmann, R. Rammal, J. Phys. Lett. 46 (1985) L173.
[20] A. Mainou, N.G. Fytas, M. Weigel, J. Phys. Conf. Ser. 2207 (1) (2022) 012009.
[21] A.A. Middleton, D.S. Fisher, Phys. Rev. B 65 (13) (2002) 134411.
[22] B. Ahrens, A.K. Hartmann, Phys. Rev. B 83 (1) (2011) 014205.
[23] J.D. Stevenson, M. Weigel, Europhys. Lett. 95 (2011) 40001.
[24] N.G. Fytas, V. Martín-Mayor, Phys. Rev. Lett. 110 (22) (2013) 227201.
[25] N.G. Fytas, V. Martín-Mayor, M. Picco, N. Sourlas, Phys. Rev. Lett. 116 (22) (2016) 227201.
[26] Y. Boykov, O. Veksler, R. Zabih, IEEE Trans. Pattern Anal. Mach. Intell. 23 (11) (2001) 1222–1239.
[27] M. Kumar, R. Kumar, M. Weigel, V. Banerjee, W. Janke, S. Puri, Phys. Rev. E 97 (2018) 053307.
[28] Y. Boykov, V. Kolmogorov, IEEE Trans. Pattern Anal. Mach. Intell. 26 (2004) 1124–1137.
[29] V. Kolmogorov, IEEE Trans. Pattern Anal. Mach. Intell. 28 (10) (2006) 1568–1583.

Table 2
Extrapolated $[m]^*$ and $[e_J]^*$ as well as the exponents b and d for the regular samples for $q = 3$ and $q = 4$, and for various system sizes N. The numbers in parentheses are the error estimates on the last significant figures.

N	$q = 3$				$q = 4$			
	$[m]^*$	$[e_J]^*$	b	d	$[m]^*$	$[e_J]^*$	b	d
16^3	0.466(48)	−2.418(26)	0.018	0.51(12)	0.69(14)	−2.54(12)	0.0163	0.31(9)
24^3	0.265(45)	−2.384(15)	0.026	0.55(8)	0.40(10)	−2.387(57)	0.0192	0.42(8)
32^3	0.145(46)	−2.369(12)	0.02	0.55(6)	0.388(94)	−2.409(52)	0.0193	0.34(6)

[30] D. Blankschtein, Y. Shapir, A. Aharony, Phys. Rev. B 29 (1984) 1263–1267.
[31] Y.Y. Goldschmidt, G. Xu, Phys. Rev. B 32 (1985) 1876–1879.
[32] K. Eichhorn, K. Binder, Europhys. Lett. 30 (6) (1995) 331.
[33] A.K. Hartmann, H. Rieger, Optimization Algorithms in Physics, Wiley, Berlin, 2002.
[34] A. Gibbons, Algorithmic Graph Theory, Cambridge University Press, Cambridge, 1985.
[35] F.Y. Wu, Rev. Mod. Phys. 54 (1982) 235–268.
[36] V. Kolmogorov, IEEE Trans. Pattern Anal. Mach. Intell. 37 (5) (2014) 919–930.
[37] V. Kolmogorov, C. Rother, in: European Conference on Computer Vision, Springer, 2006, pp. 1–15.
[38] Public code repository, https://github.com/manojkmr8788/potts.
[39] M. Kumar, V. Banerjee, S. Puri, M. Weigel, Phys. Rev. Res. 4 (2022) L042041.